Materials Science in Semiconductor Processing 150 (2022) 106972

Contents lists available at ScienceDirect

Materials Science in Semiconductor Processing

journal homepage: www.elsevier.com/locate/mssp

Multilayer porous silicon spherical Mie resonator photodiodes with comb-like spectral response in the near infrared region

Roberto Fenollosa [a,*], Moises Garín [b]

[a] Instituto Universitario de Tecnología Química, CSIC-UPV, Universitat Politècnica de València, Av. dels Tarongers, València, 46022, Spain
[b] GR-MECAMAT, Universitat de Vic – Universitat Central de Catalunya (UVIC-UCC), Campus Torre dels Frares, c/ de la Laura 13, 08500, Vic, Spain

ARTICLE INFO

Keywords:
Silicon microspheres
Photocurrent
Near infrared
Mie resonances
Optoelectronic device

ABSTRACT

Silicon microsphere photodiodes constitute optoelectronic devices able to provide resonance-enhanced photocurrent not only in the visible but also in the near infrared range by virtue of their associated Mie resonances. They are synthesized by means of a bottom-up process that allows obtaining thousand of devices in a single batch. The microspheres have revealed an internal structural configuration that strongly influences the photocurrent response, thus providing an additional degree of freedom for tuning the properties of the photodiodes. Here, devices with a particular internal configuration consisting of a high porous core, a much less porous surrounding layer and a thin non-porous shell, have been studied. They yield comb like peaked photocurrent spectra that have been fitted to a Mie type model. In addition, net energy conversion at 1500 nm has been demonstrated.

1. Introduction

Silicon is a safe bet in technology because it is stable for years and non-toxic, and is the most abundant material in earth's crust after oxygen. Silicon is the material of choice in both electronics and photovoltaics industries and constitutes one of the main representatives in photonic and optoelectronic devices. However, because of its electronic configuration, silicon, as other materials, can absorb only those photons with energy above the band gap, which mainly corresponds to the visible spectrum. This limits its efficiency in photovoltaics as it can not absorb near infrared photons coming from the sun, and it restricts its applicability for the development of on-chip devices, specially those that usually require a platform able to guide light at the telecom window around 1500 nm and at the same time light to current converters at these wavelengths. In order to somehow circumvent this limitation several strategies have been undertaken in the last years with varying degree of success. They include the combination of silicon with other materials with lower band-gap like, for instance, germanium [1], the introduction of intermediate bands in the forbidden band-gap of silicon [2,3] and the use of nanotechnology with different approaches such as photonic crystals, optical resonators, optical antennas, plasmonic nanostructures and combinations thereof [4–13]. Prominent among them is the use of photonic cavities, where the light trapping phenomenon at resonant conditions has been exploited for increasing the photocurrent in optoelectronic devices. This way, photodiodes based on Fabry-Pérot [14,15] and o-ring [16,17] resonating structures built from silicon could achieve an enhanced photo-response near 1500 nm.

In this context, we demonstrated some time ago that photodiodes built into silicon microspheres yielded photocurrent when they were irradiated by near infrared light, with spectra showing pronounced peaks that were associated with Mie resonances. Efficiency measurements performed at 990 nm yielded promising results with EQE of 18% and η of 0.6%, which corresponds to a responsivity of 0.14 A/W [18]. In addition, it was shown theoretically that they also behave as optical antennae in the visible range and could achieve absorption efficiencies higher than 100%, i.e. they could absorb light corresponding to an area larger than their geometrical projected area for certain sphere diameter and wavelength ranges [19,20]. Besides these important features, silicon microsphere-based photodiodes have other remarkable advantages, such as their compactness, combining two functionalities (light filtering and detection) in a single device of a few micrometers in size (typically from 1 to 5 μm) thanks to their resonant structure, and their fabrication procedure, which is based on a bottom-up processes where thousand of micron-size photodiodes can be developed on a substrate in a single batch after the appropriate processing.

Although these silicon particles are highly spherical and they have a

* Corresponding author.
E-mail address: rfenollo@ter.upv.es (R. Fenollosa).

https://doi.org/10.1016/j.mssp.2022.106972
Received 17 May 2022; Received in revised form 23 June 2022; Accepted 11 July 2022
Available online 18 July 2022

very smooth surface, in general the obtained particle size dispersions are relatively high, of about 35%, with a significant portion of the microspheres containing some degree of porosity in the interior, often revealed by means of a Focus Ion Beam technique [18,21]. This stems from the inherently complex aerosol type synthesis method, based on the thermal decomposition of di-silane, and the non-uniform temperature distribution in the reactor. Nevertheless, we demonstrated that the temperature gradient of the precursor gas in the reactor helps sorting particles by size, thus decreasing their size dispersion locally, and yielding larger and more porous microspheres in cold spots in comparison with those of the hot ones [22].

In spite of the important results achieved in previous experiments [18], important points still remained to be properly clarified: there has not been a satisfactory fit to a theoretical model, and the IV characteristic was not studied at wavelengths below the silicon bandgap, therefore net energy conversion or output work could not be characterized in this range. In addition, the photocurrent spectrum of silicon microsphere photodiodes was not measured at visible frequencies. From a technological point of view, one could think about these micro-devices as standalone units or as integral parts of further developments involving extended areas [19]. In any case it is very important to clarify the underlying mechanisms that drive the observed phenomena, as it has been realized in other related experiments [23].

Here, taking advantage of the structural dispersion of the microspheres obtained by the synthesis method, we have focused on a deposition area where microspheres have a particular multilayer porous configuration that produces a comb like photocurrent spectra. We have been able to fit such spectra to a model related to Mie type resonances and we have demonstrated through I–V characteristics that they yield net energy conversion at wavelengths below the Si bandgap. Additionally, we show an extended characterization of the devices towards the visible range.

2. Experimental

The photodiode devices studied here were developed by depositing amorphous Si microspheres on an n + Si supporting substrate followed by an annealing process to recrystallize the particles and favour the diffusion of n-type dopants towards the microsphere and, finally, the deposition of a thin Indium Tin Oxide (ITO) layer as a metallic type contact for both poles. The directional ITO deposition procedure along with the spherical shape of the particles ensures that the top of the microsphere and the substrate are not short-circuited. A schematic of this device configuration is shown in Fig. 1 (left), and Fig. S1 of SI shows a SEM image of a microsphere in this case with evaporated gold for easier visualizing the masking effect during deposition process. More details about this procedure and a discussion about the resulting rectifying junction are in Ref. [18].

Photocurrent measurements were performed by contacting the top of the microsphere with a conducting Pt tip attached to a XYZ nanopositioner stage [Fig. 1 (right)]. Bottom contact to the microsphere was achieved through the substrate. As opposed to earlier measurements, and as an alternative to the AFM type feedback procedure, two microscope objectives perpendicularly oriented between each other were used in order to check and to ensure the tip was properly positioned. In addition, non-polarized excitation light is here totally parallel to the supporting substrate. This has the inconvenience that part of the incident energy is lost in scattering events through the substrate but, on the other hand, it allows exciting 'clean' resonant modes in the sense that their resonant planes do not coincide with the substrate at any point. Incident mono-chromatic light comes from a supercontinuum light source after having been diffracted by a grating and passed through appropriate filters for avoiding second harmonics in the different spectral regions, from the visible to the infrared. A typical excitation power of about 3 $\mu W/\mu m^2$ at a wavelength of 1200 nm with around 2 nm of linewidth was measured with a power-meter head at the sample position. The spot shape, measured by scanning the focused optical beam across a knife-edge had a rectangular shape of about 24 $\times$ 7 μm^2. However the actual power irradiating the microsphere cannot be determined and it should have a decreased value because of the scattering with the substrate, as mentioned above. Finally, transimpedance and locking amplifiers are essential elements for being able to record the small photocurrent signals.

3. Results and discussion

3.1. Photocurrent generated by NIR radiation and fit to a spherical multilayer model

Fig. 2 (a) shows the as-recorded short circuit photocurrent spectrum of a silicon microsphere device in a wavelength range below the Si band gap (Eg ~ 1100 nm). The signal is in the range of nano-amperes and the spectrum consists of well defined peaks. The peak at 1.064 nm, not fully shown, should be disregarded because it comes from the high intensity signal at the Nd Yag laser wavelength, a basic component of the supercontinuum source [see Fig. 2 (b)]. Although the excitation system provides light beyond 2000 nm, no photocurrent signal or peaks were recorded beyond this wavelength.

Our starting hypothesis here is that all the peaks of the spectrum in Fig. 2 (a) should be originated from Mie resonances of the Si microsphere. In order to confirm it, the spectrum was base-line corrected and fitted to a Mie-based model [black and red curves respectively in Fig. 3 (a)]. The model is based on the light absorption phenomenon produced by a multilayer Si sphere [Fig. 3 (b)], specifically a 3-layered sphere with a relatively high porous core (porosity, $P \approx 40\%$), a much less porous surrounding layer ($P \approx 10\%$) (layer 1) and a non-porous thin shell (layer 2). The theoretical spectrum was obtained by the summation of a series of Transversal Electric (TE) (blue curves) and Transversal Magnetic

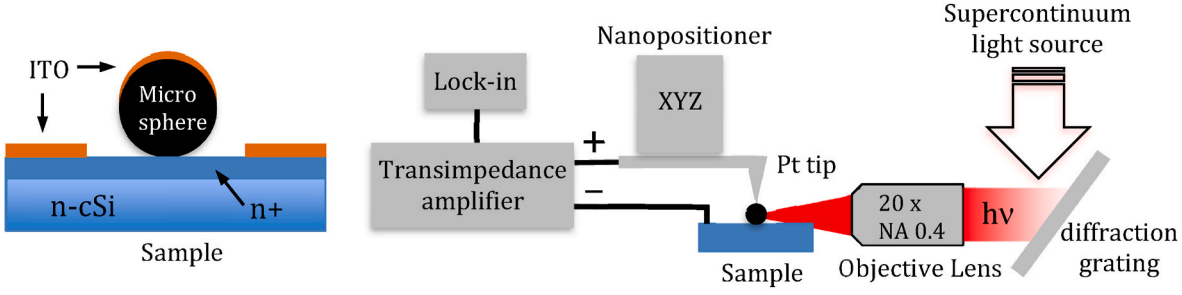

Fig. 1. Schematic of the studied silicon microsphere devices (left) and configuration for photocurrent measurements (right). The microspheres are back contacted through the substrate and front contacted by a Pt tip. Excitation monochromatic light (red areas), which irradiates the device in the direction parallel to the substrate, is obtained from a supercontinumm light source after having been diffracted by a grating. The generated current is amplified by a transimpedance and recorded via a lock-in system.

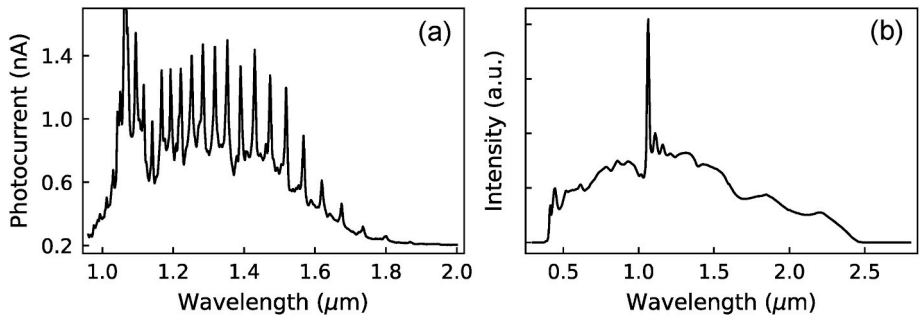

Fig. 2. a As-measured photocurrent spectrum of a silicon microsphere device in a wavelength range below the Si bandgap. **b** Spectrum of the supercontinuum source used for exciting silicon microspheres.

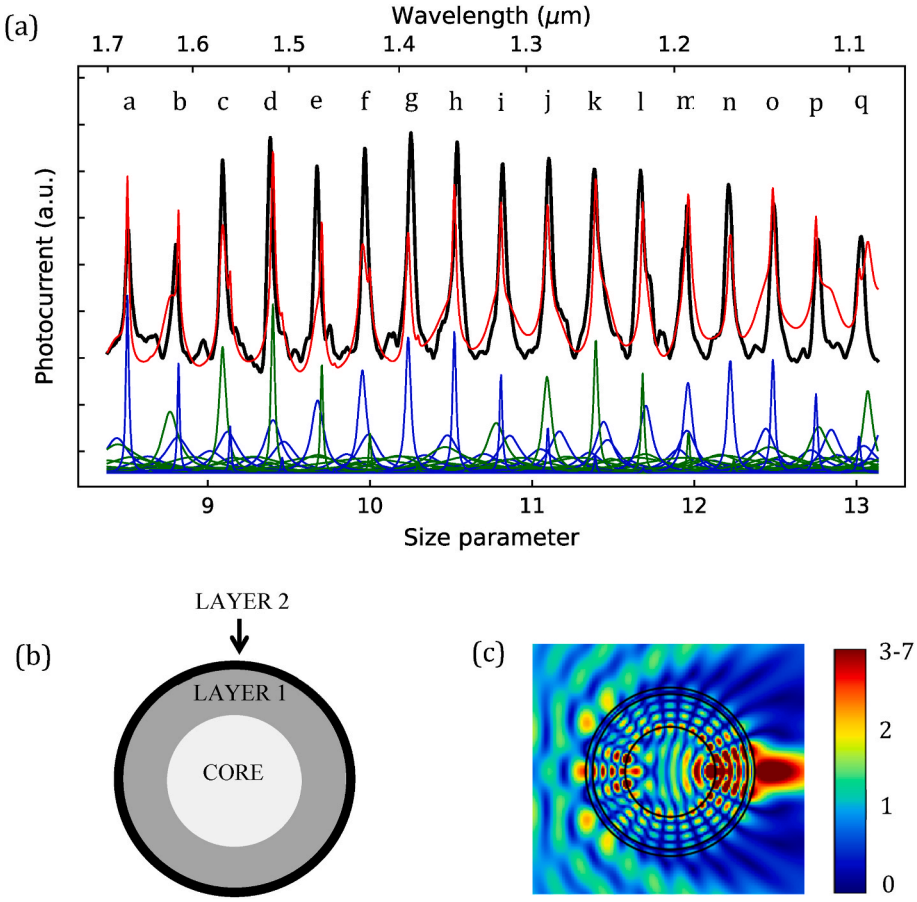

Fig. 3. a Base line corrected spectrum of Fig. 2 (black curve) and its fit to a Mie model (red curve) based on the light absorption of a three layered Si microsphere depicted in **b**, where each layer is characterized by a different porosity. The spectra have been plotted against wavelength (λ) and size parameter, defined as πΦ/λ, where Φ is the sphere diameter. The fitting spectrum (red curve) consists of the summation of a series of TE (blue curves) and TM (green curves) Mie modes. The most prominent peaks, indicated by letters, include mainly the contribution of one or several resonances and are detailed in Table 1. **c** Electric field intensity distribution for mode $TE_{12,5}$ (peak g) in the resonant plane calculated according to the algorithm detailed in Ref. [26].

(TM) (green curves) Mie modes. In general, the experimental peaks, indicated by a letter, do not always represent pure Mie resonances but they rather arise from the contribution of several nearby ones. Nevertheless, we have detailed the most contributing modes for each peak in Table 1 with the usual nomenclature [24]. Each resonant mode has a particular field distribution. As an example Fig. 3 (c) shows the electric field intensity distribution for mode $TE_{12,5}$ [letter *g* in Fig. 3 (a)] in the resonant plane. It consists of 12 intensity maxima around the half sphere perimeter and 5 maxima in the radial direction. We call this second number as radial number from now on.

The fitting model is based on the algorithm of Z. S Wu and Y. P. Wang [25] for calculating the absorption efficiency of a multilayer sphere. Some of the fitting parameters are the core diameter (Φ_{CORE}) as well as the thicknesses of layer 1 (t_{LAYER1}) and layer 2 (t_{LAYER2}). The sphere diameter can be deduced as $\Phi_{FIT} = \Phi_{CORE} + 2\,(t_{LAYER1} + t_{LAYER2})$. Other fitting parameters are related to the refractive index of the layers. Regarding the real part, it was obtained for layer 2 by interpolation between the compiled values of Palik [27] for crystalline silicon (n_{Si}) because this outer shell was assumed to be solid (non porous). Correspondingly, the porosity of the core (P_{CORE}) and layer 1 (P_{LAYER1}) were supposed to produce a decrease of their respective refractive indexes (n_{CORE} and n_{LAYER1}) according to the following equations:

$$n_{CORE} = (1 - P_{CORE})\, n_{Si} \quad (1)$$

$$n_{LAYER1} = (1 - P_{LAYER1})\, n_{Si} \quad (2)$$

Finally, the last fitting parameter is an 'apparent' imaginary part of the refractive index that we call as k_{ap} for which a single value for the whole microsphere was considered for the reasons explained below.

According to the spectrum depicted in Fig. 2 (a) the absorption of

Table 1
Transverse electric (TE) and Transverse Magnetic (TM) Mie modes associated with the peaks of Fig. 3(a).

peak	TE	TM
a	11,4	
b	12,4	10,4
c	13,4	11,4
d	9,5	12,4
e	10,5	13,4
f	11,5	14,4
g	12,5	
h	13,5	
i	14,5	12,5
j	15,5	13,5
k	11,6	14,5
l	12,6	15,5
m	13,6	16,5
n	14,6	
o	15,6	
p	16,6	14,6
q	17,6	15,6

light in the infrared region decreases at long wavelengths, vanishing near 2000 nm. Notice that the set-up provides excitation light at much longer wavelengths [Fig. 2 (b)]. Therefore, one would expect the imaginary part of the refractive index to decrease in the same way. However, this should sharpen the resonances and produce a noticeable change in that part of the spectrum but, in fact, all of the peaks have a similar linewidth. Thus, we conclude that although the absorption of light decreases at long wavelengths there is an underlying mechanism that broadens the resonances and hides the absorption phenomenon in a large part of the spectrum. We have associated this effect with the scattering of light by the porous structure of the microspheres. For this reason, the fitted parameter k_{ap} represents, in fact, an apparent imaginary part of the refractive index affected by scattering effects. Moreover, there may be other contributions to k_{ap} that do not produce useful photocurrent, like that associated to free carrier absorption due to the doping level of the microspheres.

The previous reasoning becomes clearer when considering the quality factor, Q, of the resonant peaks. It can be calculated for each resonance as $\lambda_0/\Delta\lambda$ where λ_0 is the wavelength of the peak center and $\Delta\lambda$ corresponds to its width at half maximum. As an example, peak 'g' of Fig. 3 (a) has a width of 6 nm approximately, and it results in a Q of 210. The total Q contains the contribution of several factors, according to the following equation [28].

$$\frac{1}{Q}=\frac{1}{Q_{rad}}+\frac{1}{Q_{abs}}+\frac{1}{Q_s} \tag{3}$$

where Q_{rad} is the quality factor corresponding to the intrinsic radiative (curvature) losses, Q_{abs} is associated to the material absorption contributing to the photocurrent, and Q_s includes the scattering produced by the porous structure and defects as well as any other absorption processes which do not contribute to the photocurrent, like free-carrier absorption. It is clear from eq. (3) that the total Q will be mainly determined by that process which provides the higher losses, defined by the lowest quality factor, that we think is Q_s in this case. Although it is possible to deduce theoretically the Q_{rad} value, there is no way to separate scattering and absorption contributions. Therefore, if we define the following quality factor, $Q_{abs\text{-}s}$ as:

$$\frac{1}{Q_{abs-s}}=\frac{1}{Q_{abs}}+\frac{1}{Q_s} \tag{4}$$

and taking into account the equations linking quality factor with a loss process [19,29], then:

$$Q_{abs-s}=\frac{2\pi n}{\lambda_0\alpha_{ap}} \tag{5}$$

where n is the real part of the refractive index and $\alpha_{ap}=4\pi k_{ap}/\lambda_o$ could be defined as the apparent absorption coefficient associated to k_{ap}, that includes both absorption and scattering effects.

Another argument in favour of the predominant role of the scattering concerns the type of silicon composing the microspheres. It is nanocrystalline with crystal domains of tens of nm [30]. The absorption of light below the Si band gap in this material has been related to defect states at the grain boundaries, with absorption coefficient values around 1 cm^{-1} [31–33] that corresponds to an imaginary part, k, of the order of 10^{-6}. In spite of the dopants the microspheres might have and possible contributions of the scattering itself to the absorption [34], this value is still three orders of magnitude lower than the k_{ap} values obtained by the fitting process (for instance $k_{ap}=2.52\times10^{-3}$ and correspondingly $\alpha_{ap}\approx 230$ cm^{-1} for one of the studied devices). As a result of this mismatch, absorption could be increased to some extent, for instance by hyperdoping [2,3], without destroying the resonances. This would increase, in turn, the photocurrent intensity, which is now in the range of nA. Additionally, increasing the contact areas of the microsphere with the substrate and the tip would contribute as well to improving the photocurrent. This is, however, out of the scope of this work.

In total, we measured and analysed six devices that were located around an area of about 4 mm^2. The fitted parameters are detailed in Table 2, together with the measurements of the sphere diameters by Scanning Electron Microscopy (Φ_{SEM}). Although Φ_{FIT} (the sphere diameter deduced by the fitting process) is not an actual fitting parameter it has also been detailed for the sake of comparison. It is important that they have nearly the same value in order to disregard spurious solutions of the fit. Device 1 corresponds to those spectra of Figs. 2 and 3 (a) and the spectra of the other fitted devices have been plotted in the SI.

In percentage terms with respect to the sphere diameter, all the devices have a similar configuration of core diameter, layers thicknesses and porosities. This particular combination gave rise to approximately equally spaced peaks in comb like sequences in all the measured spectra when plotted against size parameter (sp) or frequency ($sp=\pi\Phi/\lambda$ where Φ is the sphere diameter and λ is the wavelength of light). For instance, the experimental peaks in Fig. 3 (a) have a separation of nearly 0.3 in sp, which corresponds to about 50 nm at 1550 nm of wavelength. Although we have not found any rules concerning the structural configuration that allow knowing a priori when simple comb like photocurrent spectra will be obtained, several points should be commented in this regard. Firstly, small variations of the structural parameters (layers thickness and refractive index) produce significant differences in the spectra (see Fig. S12 of SI), therefore all of the layers, even the thin outer shell, contribute to the final spectral shape. Secondly, the imaginary part of

Table 2
Main fitted parameters for the photocurrent spectra of all the studied devices as well as sphere diameters deduced from the fit (Φ_{FIT}) and from the SEM measurements (Φ_{SEM}).

Device	1	2	3	4	5	6
Φ_{SEM} (nm)	4610 ±50	4300 ±50	5110 ±50	5120 ±50	4900 ±50	4360 ±50
Φ_{FIT} (nm)	4536 ±11	4310 ±10	5152 ±13	5064 ±13	4890 ±10	4270±5
Φ_{CORE} (nm)	2427 ±12	2299 ±15	2729 ±12	2635 ±12	2540 ±10	2253±6
t_{LAYER1} (nm)	852 ± 5	808 ± 5	989±4	1012 ±5	977 ± 4	813 ± 2
t_{LAYER2} (nm)	202 ± 3	199±5	223±3	202±3	198 ± 3	196±2
P_{CORE} (%)	38.31 ± 0.18	37.24 ± 0.17	37.96 ± 0.18	37.98 ±0.19	40.53 ± 0.15	40.41 ± 0.08
P_{LAYER1} (%)	8.7±0.2	7.0±0.2	8.5±0.3	10.9 ±0.3	10.6 ± 0.2	9.18 ±0.12
k_{ap} (10^{-3})	2.52 ± 0.13	2.82 ± 0.12	4.01 ±0.16	2.25 ±0.16	1.87 ± 0.09	2.51 ±0.05

the refractive index determines which modes provide a higher contribution to the absorption of light according to the *Q*-matching condition [19] ($Q_{abs\text{-}s=}Q_{rad}$). The fitted k_{qp} values favours absorption by peaks that correspond to electromagnetic field distributions with several maxima in the radial direction. However the discontinuities in the refractive index produced by the core and the non-porous shell blur the modes, specially those with high radial number, thus decreasing the number of pronounced peaks that otherwise, in a continuous solid sphere, would arise.

Perhaps a more sophisticated model that includes a higher number of layers or even a smooth transition between them would have rendered theoretical spectra closer to the experiments. However, for the sake of simplicity we have chosen the 3-layer model. Fewer layers did not fit adequately the experimental data. On another hand, other structural configurations could probably fit those spectra corresponding to microsphere photodiodes that were located in other regions of the substrate and that were measured previously [18]. Although the images of Fig. 4, acquired by high-resolution transmission electron microscopy (HRTEM), of the inner surface do not correspond exactly to a microsphere of the current studied area, they illustrate the type of structural configurations we are referring to. In this case, 4 different regions could be distinguished: a relatively large core with pores of about 100 nm in size and undetermined shape, two surrounding layers with rounded pores of 10 and 1 nm respectively and, finally, a non-porous shell [21].

3.2. Extended characterization to the VIS range

So far, we have analysed the behaviour of the devices in the NIR; in this section we will shift our attention to the photocurrent response in the visible range. Fig. 5 shows the extended photocurrent spectrum of device 1, normalized by the intensity of the excitation source (black curve). Notice that this curve is proportional to the responsivity of the device. In addition, the figure shows the absorption coefficient of crystalline silicon (red curve) for the sake of comparison. The normalized photocurrent intensity increases from 400 nm to around 850 nm where it reaches a maximum, as it occurs in a typical Si photodiode. Beyond that it decreases towards longer wavelengths, showing well defined peaks slightly above and well below the band gap position which correspond to the peaks of Fig. 2 (a) and Fig. 3(a). The ripple structure in the visible range comes from the excitation source and it is not related to the sample. The reason why resonant peaks do not appear at short wavelengths can be attributed to the increase of the absorption coefficient and the fact that there are no resonances approaching to the *Q*-maching condition in that wavelength range. They could be observed, however, in silicon spheres with size of the order of several hundred of nanometers that have, for instance, their fundamental modes: $TM_{1,1}$ and $TE_{1,1}$ in the visible range.

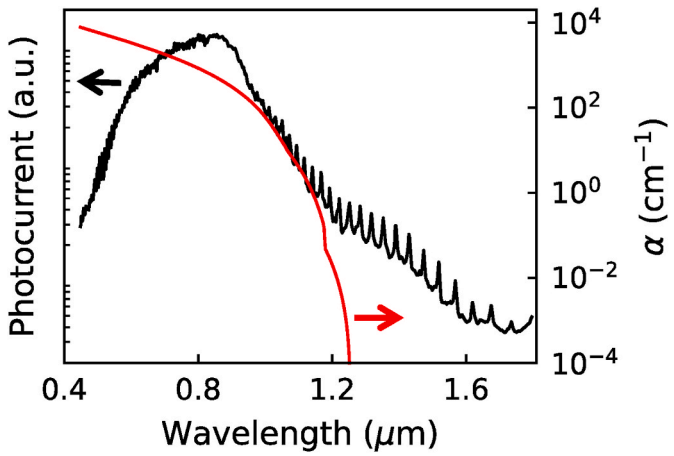

Fig. 5. Extended photocurrent spectrum of device 1 (black curve) and absorption coefficient of crystalline silicon (red curve).

We have additionally depicted the extended range photocurrent spectra corresponding to device 5 in Fig. S13 of SI.

3.3. I–V characteristic

Finally, it is important to test the behaviour of microsphere devices as diodes. For that purpose we performed measurements of the current-voltage characteristic on several devices located on the substrate area under study. Fig. 6 (a) shows one of these measurements for dark conditions (triangular points) and under monochromatic illumination at 1500 nm (round points), as well as their fit (red curves) to a non-ideal diode equation (see SI). In darkness the device shows a moderate diode rectifying behaviour whereas it clearly works as a photodiode under illumination, where it can deliver power. A detailed analysis of the I–V characteristic [Fig. 6 (b)] yielded a maximum current of 0.25 nA and a fill factor of 27% for an excitation power, measured at the head of the power-meter, of about 7 μW/μm^2. As mentioned before, however, the actual power impinging the device cannot be determined precisely and it should be much lower than that.

The differences in the I–V characteristic between dark and light conditions as well as in the fitted parameters, reported in the SI, not only prove the behaviour of the device as a photodiode but they also indicate that the absorption of light and the photocurrent generation induce themselves changes both in the device and in the measurement conditions. Specifically, there is a substantial decrease in the series and shunt resistances when the device is irradiated (see SI). The dependence of I–V curves on light intensity is a well known effect in a-Si p-i-n photodiodes

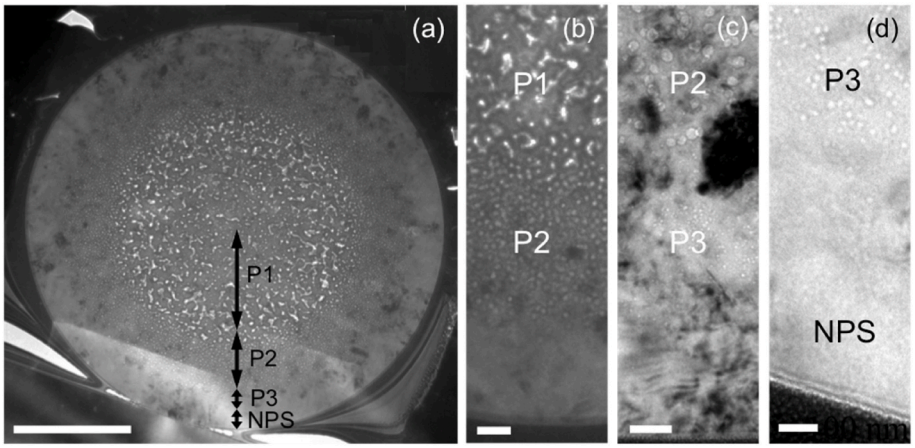

Fig. 4. a HRTEM image of the internal surface of a crystallized silicon microsphere. Different regions characterized by distinct pore sizes: P1, P2, and P3, as well as the non-porous shell (NPS) are indicated. **b** Zoomed area of **a** for better visualizing the transition between P1 and P2. **c** and **d** Higher-magnification images illustrating the transition between P2–P3 and P3-NPS, respectively. The scale bars correspond to 1 μm (**a**), 100 nm (**b**), 50 nm (**c**), and 20 nm (**d**). Reproduced from Ref. [21] with permission.

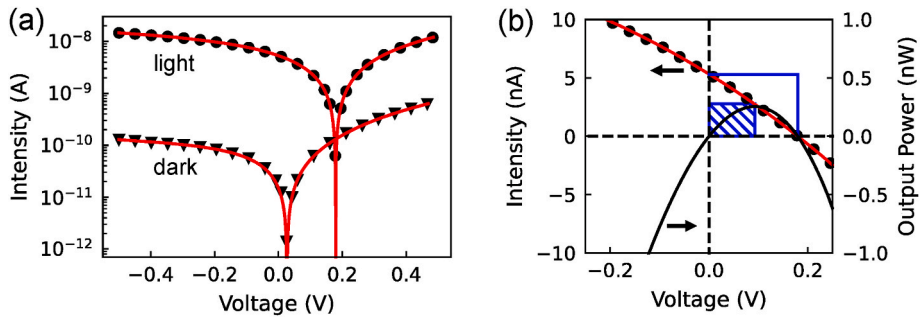

Fig. 6. a Measured current-voltage, I–V, characteristic of a silicon microsphere device in dark (triangular points) and under irradiation with monochromatic light at 1500 nm (round points) and their fit to a non-ideal diode equation (red curves). **b** Detail of the I–V curve in **a** with light irradiation for fill factor (hatched blue area) evaluation purposes. The black line corresponds to the output power calculated by using the interpolated data.

[35–37]. This seems to suggest that drift is the main collection mechanism in the devices, implying a low doping in most of the sphere volume as initially assumed [18]. Also, it would indicate that recombination due to the high density-of-states, both in the volume and in the surface of the sphere, has an important role. Improved device models for p-i-n structures might lead to more consistent results; however, the detailed study of the light-dependent I–V characteristic is beyond the scope of this work. In addition, as current increases there might also be unavoidable changes in the contact between tip and microsphere associated to the fact that no AFM type feedback control of the tip position was used for these experiments.

The I–V curves of Fig. 6 (a) and (b) do not correspond to any prominent photocurrent peak. Nevertheless, measurements of the I–V characteristics at a wavelength coinciding with a peak center did not show significant differences beyond the short-circuit current. This is not surprising because the spectral baseline is composed by the contribution of many resonances [see Fig. 3 (a)] and all in all the absorption of light is expected to occur through any of them.

4. Conclusions

Photodiodes based on silicon microspheres with an internal porous multilayer structure can absorb light and produce photocurrent and net energy conversion in the near infrared, below the silicon bandgap, at wavelengths of up to 2000 nm. The internal structure of the microspheres as well as the light scattering by the pores strongly influences the photocurrent giving rise, for some particular configurations, to comb like spectra. This provides another degree of freedom that can be used for engineering NIR optoelectronic devices based completely on silicon.

CRediT authorship contribution statement

Roberto Fenollosa: Writing – review & editing, Writing – original draft, Visualization, Validation, Supervision, Software, Resources, Project administration, Methodology, Investigation, Funding acquisition, Formal analysis, Data curation, Conceptualization. **Moises Garín:** Writing – review & editing, Validation, Supervision, Resources, Methodology, Investigation, Conceptualization.

Declaration of competing interest

The authors declare that they have no known competing financial interests or personal relationships that could have appeared to influence the work reported in this paper.

Data availability

Data will be made available on request.

Acknowledgements

This work was supported by several projects of the Spanish Ministry of Science, Innovation and Universities: PGC2018-099744-B-100 and SEV-2016-0683 from Severo Ochoa program for Centers of excellence.

Appendix A. Supplementary data

Supplementary data to this article can be found online at https://doi.org/10.1016/j.mssp.2022.106972.

References

[1] G. Sun, F. Chang, R.A. Soref, High efficiency thin-film crystalline Si/Ge tandem solar cell, Opt Express 18 (2010) 3746–3753, https://doi.org/10.1364/OE.18.003746.
[2] C. Li, J.-H. Zhao, Z.-G. Chen, Infrared absorption and sub-bandgap photo-response of hyperdoped silicon by ion implantation and ultrafast laser melting, J. Alloys Compd. 883 (2021), 160765, https://doi.org/10.1016/j.jallcom.2021.160765.
[3] J.-H. Zhao, X.-B. Li, Q.-D. Chen, Z.-G. Chen, H.-B. Sun, Ultrafast laser-induced black silicon, from micro-nanostructuring, infrared absorption mechanism, to high performance detecting devices, Mater. Today Nano 11 (2020), 100078, https://doi.org/10.1016/j.mtnano.2020.100078.
[4] K.X. Wang, Z. Yu, V. Liu, Y. Cui, S. Fan, Absorption enhancement in ultrathin crystalline silicon solar cells with antireflection and light-trapping nanocone gratings, Nano Lett. 12 (2012) 1616–1619, https://doi.org/10.1021/nl204550q.
[5] G. Kang, H. Park, D. Shin, S. Baek, M. Choi, D.-H. Yu, K. im, W.J. Padilla, Broadband light-trapping enhancement in an ultrathin film a-Si absorber using whispering gallery modes and guided wave modes with dielectric surface-textured structures, Adv. Mater. 25 (2013) 2617–2623, https://doi.org/10.1002/adma.201204596.
[6] E.C. Garnett, B. Ehrler, A. Polman, E. Alarcon-Llado, Photonics for photovoltaics: advances and opportunities, ACS Photonics 8 (2021) 61–70, https://doi.org/10.1021/acsphotonics.0c01045.
[7] S. Nunomura, A. Minowa, H. Sai, M. Kondo, Mie scattering enhanced near-infrared light response of thin-film silicon solar cells, Appl. Phys. Lett. 97 (2010), 063507, https://doi.org/10.1063/1.3478465.
[8] J. Grandidier, D.M. Callahan, J.N. Munday, H.A. Atwater, Light absorption enhancement in thin-film solar cells using whispering gallery modes in dielectric nanospheres, Adv. Mater. 23 (2011) 1272–1276, https://doi.org/10.1002/adma.201004393.
[9] L. Cao, P. Fan, A.P. Vasudev, J.S. White, Z. Yu, W. Cai, J.A. Schuller, S. Fan, M. L. Brongersma, Semiconductor nanowire optical antenna solar absorbers, Nano Lett. 10 (2010) 439–445, https://doi.org/10.1021/nl9036627.
[10] L. Cao, J.S. White, J.-S. Park, J.A. Schuller, B.M. Clemens, M.L. Brongersma, Engineering light absorption in semiconductor nanowire devices, Nat. Mater. 8 (2009) 643–647, https://doi.org/10.1038/nmat2477.
[11] M. Brongersma, Y. Cui, S. Fan, Light management for photovoltaics using high-index nanostructures, Nat. Mater. 13 (2014) 451–460, https://doi.org/10.1038/nmat3921.
[12] P. Krogstrup, H.I. Jorgensen, M. Heiss, O. Demichel, J.V. Holm, M. Aagesen, J. Nygard, A. Fontcuberta I Morral, Single-nanowire solar cells beyond the Shockley-Queisser limit, Nat. Photonics 7 (2013) 306–310, https://doi.org/10.1038/nphoton.2013.32.
[13] W.R. Erwin, H.F. Zarick, E.M. Talbert, R. Bardhan, Light trapping in mesoporous solar cells with plasmonic nanostructures, Energy Environ. Sci. 9 (2016) 1577–1601, https://doi.org/10.1039/C5EE03847B.
[14] M. Casalino, L. Sirleto, L. Moretti, M. Gioffrè, G. Coppola, I. Rendina, Silicon resonant cavity enhanced photodetector based on the internal photoemission effect at 1.55 μm: fabrication and characterization, Appl. Phys. Lett. 92 (2008), 251104, https://doi.org/10.1063/1.2952193.

[15] M. Casalino, Design of resonant cavity-enhanced Schottky graphene/silicon photodetectors at 1550 nm, J. Lightwave Technol. 36 (2018) 1766–1774, https://doi.org/10.1109/JLT.2018.2791720.
[16] D.F. Logan, K.J. Murray, J.J. Ackert, P. Velha, M. Sorel, R.M. De La Rue, P. E. Jessop, A.P. Knights, Analysis of resonance enhancement in defect-mediated silicon micro-ring photodiodes operating at 1550 nm, J. Opt. 13 (2011), 125503, https://doi.org/10.1088/2040-8978/13/12/125503.
[17] H. Zhu, L. Zhou, R. Yang, X. Li, J. Chen, Enhanced near-infrared photodetection with avalanche gain in silicon microdisk resonators integrated with p-n diodes, Opt. Lett. 39 (2014) 4525–4528, https://doi.org/10.1364/OL.39.004525.
[18] M. Garín, R. Fenollosa, R. Alcubilla, L. Shi, L.F. Marsal, F. Meseguer, All-silicon spherical-Mie-resonator photodiode with spectral response in the infrared región, Nat. Commun. 5 (2014) 3440, https://doi.org/10.1038/ncomms4440.
[19] M. Garín, R. Fenollosa, P. Ortega, F. Meseguer, Light harvesting by a spherical silicon microcavity, J. Appl. Phys. 119 (2016), 33101, https://doi.org/10.1063/1.4940047.
[20] C.F. Bohren, How can a particle absorb more than the light incident on it? Am. J. Phys. 51 (4) (1983) 323–327, https://doi.org/10.1119/1.13262.
[21] R. Fenollosa, M. Garín, F. Meseguer, Spherical silicon photonic microcavities: from amorphous to polycrystalline, Phys. Rev. B 93 (2016), 235307, https://doi.org/10.1103/PhysRevB.93.235307.
[22] M. Garín, R. Fenollosa, L. Kowalski, In situ size sorting in CVD synthesis of Si microspheres, Sci. Rep. 6 (2016), 38719, https://doi.org/10.1038/srep38719.
[23] R. Fenollosa, F. Ramiro-Manzano, M. Garín, R. Alcubilla, Thermal emission of silicon at near-infrared frequencies mediated by Mie resonances, ACS Photonics 6 (2019) 3174–3179, https://doi.org/10.1021/acsphotonics.9b01513.
[24] C.F. Bohren, D.R. Huffman, Absorption and Scattering of Light by Small Particles, John Wiley & Sons, New York, 1998, pp. 83–129.
[25] Z.S. Wu, Y.P. Wang, Electromagnetic scattering for multi-layered sphere: recursive algorithms, Radio Sci. 26 (1991) 1393–1401, https://doi.org/10.1029/91RS01192.
[26] K. Ladutenko, U. Pal, A. Rivera, O. Peña-Rodríguez, Mie calculation of electromagnetic near-field for a multilayered sphere, Comput. Phys. Commun. 214 (2017) 225–230, https://doi.org/10.1016/j.cpc.2017.01.017.
[27] E. Palik, Handbook of Optical Constants of Solids, vol. 1, Academic Press, New Yor, 1985.
[28] M.L. Gorodetsky, A.A. Savchenkov, V.S. Ilchenko, Ultimate Q of optical microsphere resonators, Opt. Lett. 21 (1996) 453–455, https://doi.org/10.1364/OL.21.000453.
[29] B.E.A. Saleh, M.C. Teich, Fundamentals of Photonics, John Wiley & Sons, 1991, p. 321.
[30] F. Meseguer, R. Fenollosa, I. Rodríguez, E. Xifré-Pérez, F. Ramiro-Manzano, M. Garín, M. Tymczenko, Silicon colloids: a new enabling nanomaterial, J. Appl. Phys. 109 (2011), 102424, https://doi.org/10.1063/1.3581880.
[31] Tsvetelina Merdzhanova, Thesis Microcrystalline Silicon Films and Solar Cells Investigated by Photoluminescence Spectroscopy, Bulgarian Acdemy of Sciences, Sofia, 2004.
[32] M.R. Esmaelili-Rad, A. Sazonov, A.G. Kazanskii, A.A. Khomich, A. Nathan, Optical properties of nanocrystalline silicon deposited by PECVD, J. Mater. Sci. Mater. Electron. 18 (2007) 405–409, https://doi.org/10.1007/s10854-007-9230-8.
[33] R. Carius, F. Finger, U. Backhausen, M. Luysberg, P. Hapke, M. Otte, H. Overhof, Electronic properties of microcrystalline silicon, MRS Symp. Proc. 467 (1997) 283, https://doi.org/10.1557/PROC-467-283.
[34] A. Poruba, A. Fejfar, Z. Remes, J. Springer, M. Vanecek, J. Kocka, J. Meier, P. Torres, A. Shah, Optical absorption and light scattering in microcrystalline silicon thin films and solar cells, J. Appl. Phys. 88 (2000) 148–160, https://doi.org/10.1063/1.373635.
[35] J. Merten, J.M. Asensi, C. Voz, A.V. Shah, R. Platz, J. Andreu, Improved equivalent circuit and analytical model for amorphous silicon solar cells and modules, IEEE Trans. Electron. Dev. 45 (1998) 423–429, https://doi.org/10.1109/16.658676.
[36] P. Löper, M. Canino, D. Qazzazie, M. Schnabel, M. Allegrezza, C. Summonte, S. W. Gluz, S. Janz, M. Zacharias, Silicon nanocrystals embedded in silicon carbide: Investigation of charge carrier transport and recombination, Appl. Phys. Lett. 102 (2013), 033507, https://doi.org/10.1063/1.4789441.
[37] S.S. Hegedus, Current-voltage analysis of a-Si and a-SiGe solar cells including voltage-dependent photocurrent collection, Prog. Photovoltaics Res. Appl. 5 (1997) 151–168, https://doi.org/10.1002/(SICI)1099-159X(199705/06)5:3<151::AID-PIP167>3.0.CO;2-W.